AGU PUBLICATIONS

Geophysical Research Letters

RESEARCH LETTER
10.1002/2015GL066764

Key Points:
- Surface evaporation biases contribute as much as cloud biases to the warm bias intensity
- Biases in surface humidity explain most of the evaporation biases over the eastern tropical oceans
- Evaporation and relative humidity control the response of the surface temperature to heat fluxes

Supporting Information:
- Supporting Information S1

Correspondence to:
F. Hourdin,
frederic.hourdin@lmd.jussieu.fr

Citation:
Hourdin, F., A. Găinuşă-Bogdan, P. Braconnot, J.-L. Dufresne, A.-K. Traore, and C. Rio (2015), Air moisture control on ocean surface temperature, hidden key to the warm bias enigma, *Geophys. Res. Lett.*, *42*, doi:10.1002/2015GL066764.

Received 26 OCT 2015
Accepted 1 DEC 2015
Accepted article online 11 DEC 2015

Air moisture control on ocean surface temperature, hidden key to the warm bias enigma

Frédéric Hourdin[1], Alina Găinusă-Bogdan[2], Pascale Braconnot[2], Jean-Louis Dufresne[1], Aboul-Khadre Traore[1], and Catherine Rio[1]

[1]Laboratoire de Météorologie Dynamique/IPSL/UPMC Univ Paris 06/Sorbone Universités/CNRS, Paris, France, [2]Laboratoire des Sciences du Climat et de l'Environnement, IPSL, unité mixte CEA-CNRS-UPS, Gif sur Yvette, France

Abstract The systematic overestimation by climate models of the surface temperature over the eastern tropical oceans is generally attributed to an insufficient oceanic cooling or to an underestimation of stratocumulus clouds. We show that surface evaporation contributes as much as clouds to the dispersion of the warm bias intensity in a multimodel simulations ensemble. The models with the largest warm biases are those with the highest surface heating by radiation and lowest evaporative cooling in atmospheric simulations with prescribed sea surface temperatures. Surface evaporation also controls the amplitude of the surface temperature response to this overestimated heating, when the atmosphere is coupled to an ocean. Evaporation increases with temperature both because of increasing saturation humidity and of an unexpected drying of the near-surface air. Both the origin of the bias and this temperature adjustment point to the key role of near-surface relative humidity and its control by the atmospheric model.

1. Introduction

The coupling of global atmospheric and oceanic general circulation models in the 1980s and 1990s was a main step toward the emergence of the global climate models or Earth System Models which are now used to estimate climate changes caused by anthropogenic and natural perturbations [*Lynch*, 2008; *Edwards*, 2010]. Generally, the atmospheric model computes the radiative and turbulent surface fluxes which are communicated as a top boundary condition to the oceanic model which then returns a surface temperature as a boundary condition for the atmospheric model. The good representation of the atmosphere/ocean coupling depends on the skill of both components to represent the explicit dynamics as well as, through parameterizations, the turbulence and clouds which strongly affect the heat fluxes at the surface. The evaluation of global climate models and their use for climate change projections is nowadays strongly coordinated at an international level via the Coupled Model Intercomparison Project (CMIP) [*Taylor et al.*, 2012]. Beyond their use for prediction at meteorological to climatic timescales, global models play a key role in climate science. They are essential to understand and assess the mechanisms at work in the climate system accounting for all the complexity and spatial and temporal scales involved [*Dahan Dalmedico*, 2001; *Held*, 2005].

Despite significant improvements in the representation of several aspects of the climate system over the years [*Reichler and Kim*, 2008], certain systematic errors continue to elude decades of research to explain their origin. In particular, most state-of-the-art climate models overestimate the surface temperature over the eastern tropical oceans by a few degrees [*Richter*, 2015; *Vannière et al.*, 2014]. The persistence of this systematic bias was confirmed in the Intergovernmental Panel on Climate Change Fifth Assessment Report [*Flato et al.*, 2013], and the fact that it did not reduce between two consecutive phases of the CMIP exercise separated by 7 years was felt to be a significant failure by the climate modeling community [*Zheng et al.*, 2011; *Xu et al.*, 2014a]. This long-standing bias casts some doubts on the reliability of future projections for climate systems that crucially depend on ocean temperature, such as the West African monsoon [*Roehrig et al.*, 2013], and highlights a poor understanding of the processes controlling the energy balance at the air-sea interface.

So far this warm bias has been attributed to insufficient cold water upwelling due to deficiencies in the representation of either ocean mixing or atmospheric wind stresses [*Xu et al.*, 2014a; *Zheng et al.*, 2011] and to the underrepresentation of the banks of stratocumulus clouds [*Ma et al.*, 1996; *Yu and Mechoso*, 1999; *de Szoeke et al.*, 2010; *Richter*, 2015] covering these cold water areas. We show here that biases in surface evaporation, which were not considered so far, play as strong a role as cloud radiative effects in controlling the intensity

of the warm bias in the CMIP5 simulations. To show this, we introduce in section 2 an Eastern Tropical Ocean Anomaly (ETOA) index and use it in section 3 to analyze the relationship between energy flux anomalies in stand-alone atmospheric simulations and the sea surface temperature bias in coupled atmosphere-ocean simulations. We then show in section 4 how evaporation dominates the response of sea surface temperature to anomalies in the surface energy fluxes. Based on a decomposition of the latent heat flux response, we finally show in section 5 the role played by surface humidity in both the original forcing of the warm biases and the response of evaporation, before deriving our conclusions in section 6.

2. The ETO Warm Bias in CMIP5

We base our analysis on 20 models that participated to CMIP5 [*Taylor et al.*, 2012] and for which the latent heat flux (*LE*), sensible heat flux (*H*), and surface radiation (SW and LW) were available for both coupled ocean-atmosphere "historical" simulations and stand-alone "amip" atmospheric simulations with prescribed sea surface temperature (SST). All the diagnostics presented here concern the 1979–2005 climatological annual mean. All the simulations are reduced to a common $3.75 \times 2.5°$ grid with a selective air-sea mask chosen to avoid island or coastal effects, which may contaminate the fields differently in the observations and in the models.

We show in Figure 1a the mean error pattern in the ensemble mean of the CMIP5 historical coupled ocean-atmosphere simulations. The error is computed with respect to the sea surface temperature used as a boundary condition in the amip stand-alone atmospheric simulations. The tropical mean error is removed to retain only the error in the spatial pattern. The SST bias pattern clearly shows the regions of systematic warm biases on the eastern tropical oceans (ETO).

To focus on these particular biases, an ETO anomaly (ETOA) is defined for any variable as the difference between the mean value of the variable over an ETO mask (i.e., considering all the oceanic grid points inside the red contours in Figures 1a–1d) and over the full tropical oceans. The red contour itself corresponds to a 0.8 K threshold value for the sea surface temperature biases in the CMIP5 ensemble mean. The SST bias has a clear interhemispheric signature featuring a too cold Northern Hemisphere. Since this aspect of the bias is not the focus of this study, the zonal mean was removed before applying the 0.8 K threshold. Throughout the paper, this departure from the zonal mean is used only to define this mask and is not present in any of the calculations. This rather arbitrary choice does not affect the results, as illustrated in the supporting information Figure S2.

The sea surface temperature bias ETOA is given in Kelvin in parenthesis for the 20 models considered: CSIRO-Mk3-6-0 (−0.28), ACCESS1-3 (0.75), CESM1-CAM5 (0.76), ACCESS1-0 (0.89), bcc-csm1-1-m (0.98), CCSM4 (1.31), IPSL-CM5A-MR (1.37), MRI-CGCM3 (1.52), GISS-E2-R (1.53), MPI-ESM-LR (1.54), MPI-ESM-MR (1.55), MIROC5 (1.56), IPSL-CM5A-LR (1.58), GFDL-CM3 (1.59), BNU-ESM (1.68), NorESM1-M (1.85), CNRM-CM5 (1.86), IPSL-CM5B-LR (1.93), FGOALS-s2 (1.96), and FGOALS-g2 (2.06). More information on the individual models can be found in the Intergovernmental Panel on Climate Change Chapter on model evaluation [*Flato et al.*, 2013]. All but one model (i.e., CSIRO) feature a temperature bias ETOA larger than 0.7 K, with an ensemble average of 1.4 K.

3. Atmosphere Forcing the ETOA Bias

The contrast between the coverage by the banks of stratocumulus clouds over the ETO region and by trade-wind cumulus in the rest of the tropics, sketched in Figure 2b, induces a contrast in the shadowing effect of clouds, less short-wave radiation reaching the surface over the ETO. The main reason invoked to explain the atmospheric contribution to the ETO warm bias so far was the underestimation of the occurrence (or lack) of these stratocumulus clouds. Despite dedicated research efforts and ad hoc treatment to increase their occurrence [*Hourdin et al.*, 2013a], significant biases in the cloud radiative effect persist in stand-alone atmospheric simulations forced by observed sea surface temperatures. This is illustrated in Figure 1b which shows the pattern of the cloud radiative effect bias in the CMIP5 ensemble mean computed with respect to the CERES-EBAF data set [*Loeb et al.*, 2009]. For most models, the overestimated surface radiation in the ETO region is mainly due to short-wave radiation and is a consequence of an underestimated cloud cover. In a few of them, however, the cloud cover is well simulated, but the cloud base is too low and thus too warm, which leads to an overestimated downward long-wave radiation toward the surface (or greenhouse effect).

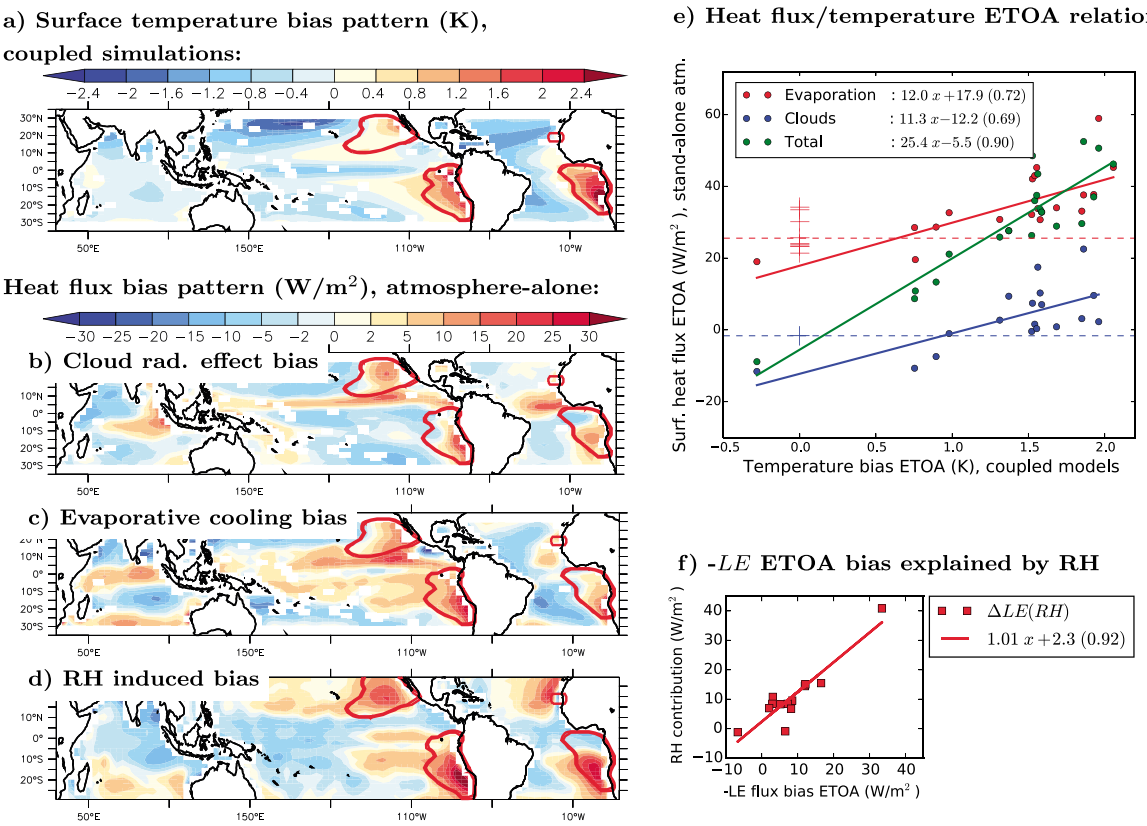

Figure 1. Relationship between the patterns of ocean surface temperature bias in coupled CMIP5 historical simulations and flux biases in stand-alone amip atmospheric simulations. (a) Mean sea surface temperature bias (in K) in coupled ocean-atmosphere CMIP5 simulations, computed over the period 1979–2005 for 20 models. The tropical average is removed to focus on bias patterns. (b–d) Patterns of surface atmospheric heat flux biases (W/m^2) obtained in stand-alone atmospheric simulations for (Figure 1b) the cloud radiative effect computed as the difference between the all-sky and the clear-sky radiative flux, (Figure 1c) the latent heat flux, and (Figure 1d) the contribution of the relative humidity mean bias to the latent heat bias (see text). Biases are computed using as observational references: the climatological mean of the SST data set used as boundary condition for the amip simulations [*Taylor et al.*, 2000], the second edition of the CERES-EBAF L3b product for radiative fluxes [*Loeb et al.*, 2009], the ensemble mean of 11 in situ, satellite-based, and blended climatological products for latent heat fluxes [*Găinuşă-Bogdan et al.*, 2015] and the *da Silva et al.* [1994] climatology for relative humidity. (e and f) We consider the ETO anomaly (ETOA) of SSTs biases and atmospheric fluxes. The ETOA is computed as the difference of the mean value of a quantity over an ETO mask (i.e., inside the red contours in Figures 1a–1d) and over the full tropical oceans (from 30°S to 30°N). (e) Scatterplot of atmospheric fluxes ETOA as a function of the ocean temperature bias ETOA for cloud radiative effect (blue), for latent heat (red), and for the total surface heat flux (i.e., total radiation plus latent and sensible heat fluxes). Numerical values are given in Table S1 in the supporting information. Equations of the regression lines (full lines) and correlation coefficients are given in the legend. The red and blue horizontal dashed lines show the mean observed ETOA, and the plus signs show the individual observational estimates (see text). (f) Scatterplot of the contribution of the relative humidity bias ETOA to the latent heat flux bias ETOA. For the cloud radiative effect in Figures 1b and 1e, results of CESM1-CAM5 and FGOALS-g2 were ignored due to missing clear-sky fluxes. For Figure 1d, the decomposition used requires in addition near-surface humidity, wind, and air temperature. For these figures, the bcc-csm1-1-m, CCSM4, CESM1-CAM5, FGOALS-g2, MPI-ESM-LR, MPI-ESM-MR, and NorESM1-M models were ignored because one of these variables was missing (see supporting information Table S2 for details). The comparison of the 13 and 18 model ensemble is given in the supporting information Figure S1.

The role of the underestimation of surface evaporation in these regions, compared to the mean evaporation over the tropical oceans, is less acknowledged in the literature. Indeed, the bias pattern of evaporative cooling $-LE$ (counted positively downward, L being the water latent heat of vaporization and E the surface evaporation) in stand-alone simulations (Figure 1c) shows strong similarities with the temperature bias pattern obtained when the same atmospheric models are coupled to an ocean model (Figure 1a).

This result should be taken with caution, however. Even if the confidence in evaporation climatologies at the ocean surface has recently increased [*Yu and Weller*, 2007; *de Szoeke et al.*, 2010], the surface flux observations used as a reference for bias computations still exhibit large uncertainties. In this paper, the choice of observations of turbulent fluxes is based on a recent overview of available data [*Găinuşă-Bogdan et al.*, 2015]. The observational reference used to compute the latent heat flux bias in Figure 1c is the ensemble mean of a set of 11 in situ, satellite-based, and blended climatological air-sea flux products.

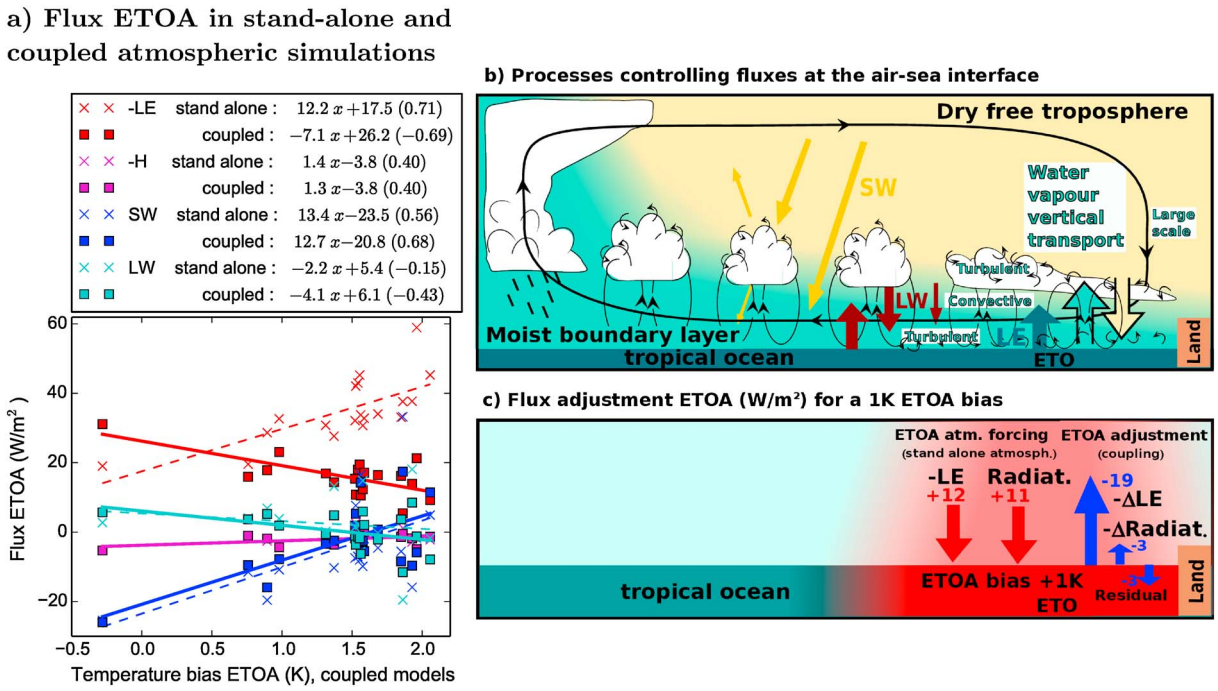

Figure 2. Adjustment between fluxes in atmosphere-alone simulations and temperature in coupled simulations. (a) Multimodel scatterplot of the atmospheric flux ETOA (in W/m^2) in stand-alone atmospheric (crosses and dashed regression lines) and ocean-atmosphere coupled (squares and full lines) simulations as a function of the temperature bias ETOA in coupled simulations. Fluxes are decomposed into latent (−*LE*) and sensible (−*H*) heat flux and short-wave (SW) and long-wave (LW) radiation. The results of ACCESS1-3 were ignored due to missing upward radiation in the historical simulation. (b) Sketch of the main processes involved in the control of air-sea fluxes, illustrating the control of SW and LW radiation by clouds as well as the various components of the water vapor transport controlling the near-surface humidity and the evaporation. (c) Summary of the atmospheric fluxes ETOA at the origin of the warm bias (stand-alone simulations; red arrows) and of the response of the surface fluxes to this temperature bias (difference between coupled and stand-alone simulations; blue arrows). The numerical values are deduced from the slopes of the regression lines of Figure 2a and are given in W/m^2 for a 1 K SST ETOA bias.

The role of surface energy fluxes can be identified as well with no reference to flux observations, by considering directly the multimodel dispersion through the ETOA index. We plot in Figure 1e the surface heat flux ETOA in stand-alone atmospheric simulations as a function of the temperature bias ETOA in coupled atmosphere-ocean simulations for all the models. It happens that ETOAs of both cloud radiative effect (Figure 1e, blue) and latent heat flux (red) in stand-alone atmospheric simulations are correlated with the temperature bias ETOA in coupled atmosphere-ocean simulations, with mean regression slopes of 11 and 12 W/m^2/K, respectively. Together, they contribute to most of the 25 W/m^2/K slope of the total atmospheric surface flux ETOA (i.e., total radiation plus latent and sensible heat flux; Figure 1e, green). This is a strong indication that the poor representation of both clouds and evaporation in atmospheric models contribute to the warm bias.

The estimate of the cloud radiative effect ETOA from CERES-EBAF observation is shown as a blue dashed line in Figure 1e. The ensemble mean latent flux observation ETOA corresponds to the red dashed line, and the 11 individual data sets considered in the *Găinuşă-Bogdan et al.* [2015] study are also shown as red plus signs. For a null temperature bias ETOA (Figure 1e, origin of abscissa), the regression line of the latent heat and of the cloud radiative effect are both below the observations. If relying on the mean regression line and mean observation, an atmospheric model that would be bias free for the fluxes ETOA would result in a SST ETOA bias in the coupled simulations of about 0.8 K. This is indicative of either systematic errors in the observations or of an additional systematic error in models, as would result from a systematically underestimated oceanic upwelling.

Several reasons can explain why underestimated evaporative cooling has not been identified as key to ETO warm biases so far. First, it is important to identify flux biases in stand-alone atmospheric simulations. Evaporative cooling is generally overestimated over the ETO in coupled CMIP5 simulations [*Zheng et al.*, 2011; *de Szoeke et al.*, 2010; *Richter*, 2015], but a large part of this excessive cooling is the consequence, rather than the cause, of the warm biases, as it will be shown in next section. A second important methodological

aspect is to consider anomaly patterns of evaporation, rather than the absolute bias. It is done here either by removing the average from the maps (Figures 1a–1c) or by computing ETOAs (Figure 1e). Indeed, the evaporation is often overestimated in the tropics in CMIP5 stand-alone atmospheric simulations [*Xu et al.*, 2014a; *Richter*, 2015] but to a lesser extent in the ETO region. When coupling the atmospheric model with an ocean model, the mean temperature and energy fluxes adjust (the mean temperature is often fitted to the observation by tuning of the global energy balance), but the pattern of the temperature biases in coupled models clearly conserves the footprint of the flux anomalies in stand-alone atmospheric simulations.

4. Adjustment of Temperature and Fluxes

This adjustment of temperature and fluxes is now analyzed in more detail in Figure 2a which compares the ETOA fluxes in stand-alone and coupled atmospheric simulations as a function of the temperature bias. In stand-alone simulations, the surface temperature is prescribed to observations, so that its change after the coupling is equal to the bias in the coupled simulation. The short-wave radiation (SW) is almost unchanged by the coupling. The long-wave (LW) net radiation and sensible heat flux (*H*, in general 5 to 10 times smaller than *LE* over tropical oceans) are also only marginally affected by the coupling. To the first order, these fluxes depend on the contrast between the temperature at the surface and in the atmospheric column, the latter adjusting to the former, as sketched by the reddening of the ocean and atmosphere over the ETO region in Figure 2c. Finally, the surface latent heat flux controls most of the adjustment: the slope of the regression between the latent heat ETOA and the temperature bias ETOA (Figure 2a) is of opposite sign in the stand-alone (12 W/m^2/K) and in the coupled (−7 W/m^2/K) experiments, and the difference between the two slopes (19 W/m^2/K) is not far from the regression slope of the initial forcing (25 W/m^2/K; green line in Figure 1e). The adjustment overcompensates the original latent heat flux perturbation so that the flux bias ETOA is of opposite sign in stand-alone and coupled simulations. In comparison, the contribution of the sensible heat flux to the adjustment to the initial forcing is 0.2 W/m^2/K and that of the radiation (SW+LW) is 2.6 W/m^2/K. The residual of about 3 W/m^2/K can be interpreted as a slightly increased oceanic heat uptake in the ETO region. A summary of these findings is given in Figure 2c. The red arrows correspond to the main flux ETOA biases in stand-alone atmospheric simulations associated with a 1 K SST ETOA bias, as estimated from the slopes of the regression lines in Figure 2a (red dashed line for latent heat and sum of the two blue dashed lines for radiation). The blue arrows correspond to the adjustment of fluxes with temperature in coupled simulations for a 1 K change in the SST ETOA, as estimated from the differences of the regression slopes in Figure 2a between coupled and stand-alone simulations.

We now analyze further the response of the latent heat flux to temperature changes, when coupling the atmospheric and oceanic models. Latent heat flux is computed at the model time step as

$$LE = \rho L C_E |V_a| \left[\alpha q_{\mathrm{sat}}(T_s) - q_a\right] \tag{1}$$

where the specific humidity q_a is the mass of water vapor divided by the total mass of dry air plus vapor, ρ is the air density, C_E is the transfer coefficient for the evaporation, $|V_a|$ is the near-surface horizontal wind speed, $\alpha \simeq 0.98$ accounts (in some of the models) for the smaller evaporation of salty water than fresh water, and $q_{\mathrm{sat}}(T_s)$ is the specific humidity at saturation for surface temperature T_s. When the temperature increases, the evaporation increases because of the $q_{\mathrm{sat}}(T_s)$ term, but this increase can be partly compensated by the subsequent increase in air humidity q_a. This formula is rewritten by introducing the air relative humidity $\mathrm{RH}_a = q_a / q_{\mathrm{sat}}(T_a)$, by linearizing the difference $q_{\mathrm{sat}}(T_s) - q_{\mathrm{sat}}(T_a)$ as a function of the air-sea temperature contrast $\delta T = T_s - T_a$, and by using the Clausius-Clapeyron relation: $q'_{\mathrm{sat}}(T) = L/(R_v T^2) q_{\mathrm{sat}}(T)$ (see Appendix A). The latent heat flux then reads as follows:

$$LE \simeq \rho L C_E |V_a| q_{\mathrm{sat}}(T_a) \left[\alpha \frac{L}{R_v {T_a}^2} \delta T + \alpha - RH_a\right] \tag{2}$$

The temperature dependency of *LE* is more visible in this reformulation where $q_{\mathrm{sat}}(T_s)$ is factorized.

5. Decomposing the Latent Heat Flux Response

Equation (2) is now used as a bulk formula to analyze a posteriori the latent heat flux adjustment to the coupling with the ocean model, considering the climatological annual means of the near-surface variables

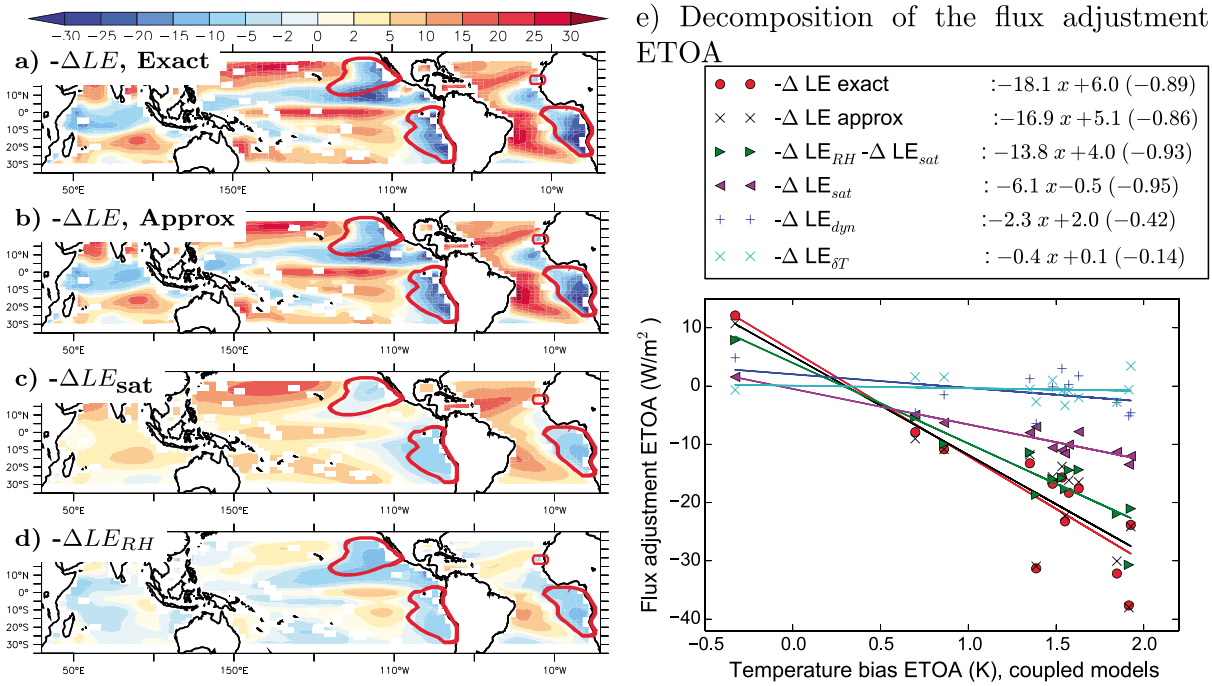

Figure 3. Decomposition of the latent heat flux adjustment ΔLE (in W/m^2) between stand-alone and coupled atmospheric simulations. The latent heat flux adjustment is approximated as the sum of four contributions, respectively, due to changes in wind speed ($\Delta LE_{\rm dyn}$), saturation humidity ($\Delta LE_{\rm sat}$), relative humidity ($\Delta LE_{\rm RH}$), and sea-air temperature contrast ($\Delta LE_{\delta T}$). (a–d) The geographical distribution of the actual and approximate flux adjustments, as well as the contributions of changes in saturation humidity and in relative humidity to this flux adjustment are shown, respectively. (e) The multimodel scatterplot of the actual and the approximate flux adjustment ETOA as well as the multimodel scatterplot of their various contributions are shown as a function of the surface temperature bias ETOA in the coupled simulations. For this figure, the same 13 models were retained as in Figure 1d.

available in the CMIP5 archive and using an effective coefficient $C_E^* = 1.4\ 10^{-3}$ and $\alpha = 1$ (see Appendix A). It allows us to decompose the latent heat adjustment to ocean coupling ΔLE (where Δ refers to the difference "coupled" minus "stand-alone") into four contributions: (1) a dynamical contribution $\Delta LE_{\rm dyn}$ associated with changes in near-surface wind speed $\Delta|V_a|$, (2) a term $\Delta LE_{\rm sat}$ associated with changes in saturation humidity with atmospheric temperature ΔT_a, (3) a term $\Delta LE_{\rm RH}$ associated with changes in relative humidity ΔRH, and (4) a term $\Delta LE_{\delta T}$ associated with changes in sea-air temperature contrast $\Delta\delta T$. The sum of these four contributions is a very good approximation of the actual latent heat flux adjustment ΔLE, as seen by comparing Figures 3a and 3b.

Figure 3e shows the ETOA of the four contributions to the total latent heat flux adjustment as a function of the SST bias ETOA: the changes in saturation humidity ($\Delta LE_{\rm sat} \approx 6$ W/m^2/K) and in relative humidity ($\Delta LE_{\rm RH} \approx 8$ W/m^2/K) are the two main contributions to the latent heat adjustment (ΔLE ≈ 18 W/m^2/K) and control the ETO adjustment when the atmosphere is coupled to the ocean (Figure 3e). Note that the difference with the 19 W/m^2/K deduced from Figure 2 comes from the different model ensembles used.

The effect of change in saturation humidity could have been anticipated: the $\Delta LE_{\rm sat}$ 6 W/m^2/K regression slope can be directly estimated by using equation (2), by taking $\beta = L/(R_v T_a^2) \simeq 0.06$ as a constant, in which case $\Delta LE_{\rm sat} \simeq \beta\ LE\ \Delta T_a$, and by considering typical LE values in the tropics of the order of 100 W/m^2. More surprisingly, the contribution of the relative humidity reinforces the contribution of the saturation, which means that the relative humidity of near-surface air temperature decreases when surface temperature increases. It is well understood that while surface evaporation moistens the boundary layer, turbulent mixing and boundary layer convection dries it out via the entrainment of dry tropospheric air [*Stevens*, 2007]. The air entrained from the free troposphere is particularly dry over the ETO, in the subsiding branches of the Hadley-Walker circulation, as sketched in Figure 2b. Specific humidity is well mixed in the boundary layer, which corresponds to a relative humidity decreasing from the cloud layer (where it is close to 1) to the

surface, with a gradient imposed by the Clausius-Clapeyron relation. Thus, an increased shallow convection and deeper boundary layer probably explain the drying of the air above the warmer surface. A similar process has been invoked [*Shkolnik et al.*, 1980] to explain how Bedouins living in desert areas, by wearing dark and loose clothes, compensate the absorption of radiation by a reinforced convection along their skin, which leads to an increased dry air renewal and a subsequent cooling by evaporation.

Beyond disentangling of the different contributions to the response of the latent heat flux to coupling, the decomposition presented above can be used to analyze the $-LE$ bias itself. In particular, it can be used to compute the contribution $\Delta LE_{\mathrm{RH}} = -\gamma^* |V_a|\, q_{\mathrm{sat}}(T_a)\Delta\mathrm{RH}$ of the relative humidity biases to latent heat biases in stand-alone atmospheric simulations. ΔRH in this case is the difference with RH observations for which we use the *da Silva et al.* [1994] climatology. The ensemble mean pattern of the RH contribution to the latent heat bias is shown in Figure 1d. The patterns are very similar to that of the effective latent heat bias (Figure 1c). Figure 1f shows for each model the RH contribution as a function of the effective latent heat bias considering the ETOA index. The slope close to unity and the correlation of 0.92 are clear indications of the dominance of the RH contribution to the latent heat bias ETOA. Although the Da Silva data set used to compute the humidity bias has its own unknown uncertainties, it is interesting noticing that the data sets used as references in Figures 1c and 1d are largely independent of each other.

6. Conclusions

Based on a multimodel analysis, we have shown that the processes controlling relative humidity and evaporation play a key role both in the forcing and in the adjustment of the ETO warm biases. The latent heat contribution to the atmospheric flux biases in stand-alone atmospheric CMIP5 models is on average a little bit larger than the contribution of clouds.

This study does not rule out other possible sources of biases, such as the representation of the oceanic circulation [*Large and Danabasoglu*, 2006], which may in particular reshape the warm bias along the coast [*Xu et al.*, 2014b] or in the equatorial regions [*Xu et al.*, 2014a]. Observational uncertainties are too large to allow quantifying the residual part of the sea surface temperature bias which could be attributed to wind-induced or internal problems in the representation of surface oceanic cooling.

By itself, the overestimated relative humidity with respect to the rest of the tropics is enough to explain the underestimated evaporation over the ETO and is probably due to an underestimated vertical exchange with the dry troposphere. As most attempts to reduce the ETO warm bias have focused on the radiative impact of stratocumulus clouds, model developers may have decreased the vertical mixing within the boundary layer or the top entrainment rate in order to maintain enough moisture to simulate a realistic coverage by stratocumulus clouds. By doing this, the short-wave radiative heating is indeed reduced, but the evaporative cooling is reduced as well. It was clearly the case in the three CMIP5 configurations of the IPSL model (supporting information Table S1). A strong and even overestimated coverage by clouds was obtained by artificially reducing the mixing in regions of strong temperature inversion at boundary layer top [*Hourdin et al.*, 2013a, 2013b]. This ad hoc treatment resulted, however, in an overestimation of the long-wave surface heating, the clouds being too low, in an overestimation of the near-surface humidity and subsequent underestimation of the surface evaporative cooling, as expected for a too thin boundary layer [*Stevens*, 2007]. As a result, these ad hoc treatments probably contributed to increase rather than decrease the ETO warm biases in the IPSL model.

Latent heat also controls 80% of the atmospheric adjustment to the flux forcing, 77% of which are due to the contributions of saturation (33%) and relative humidity (44%). The decrease of relative humidity over the ETO after coupling with ocean can be well explained by a deepening of the boundary layer in response to the surface warm bias, without ruling out other possible contributions such as an increased advection of dry air from the continents or subtropics toward the warmer SSTs, or feedbacks with the large-scale tropical circulation [*Neggers et al.*, 2007; *Braconnot et al.*, 2007].

The importance of the processes controlling the near-surface humidity and their poor representation in climate models deserve more attention, specific research, and observational programs. This conclusion is in line with the first recommendation of the European Organisation for the Exploitation of Meteorological Satellites "Climate Symposium 2014" [*Asrar et al.*, 2015].

Appendix A: Latent Heat Flux Decomposition

By introducing $\gamma = \rho C_E L$, and considering $q_a = RH q_{\text{sat}}(T_a)$ and linearizing $q_{\text{sat}}(T_s) - q_{\text{sat}}(T_a)$ as a function of $\delta T = T_s - T_a$, equation (1) for the latent heat flux reads as follows:

$$LE = \gamma\, |V_a| \left[\alpha \left. \frac{\partial q_{\text{sat}}}{\partial T} \right|_{(T=T_a)} \delta T + (\alpha - RH)\, q_{\text{sat}}(T_a) \right] \tag{A1}$$

which leads to equation (2) when using the Clausius-Clapeyron equation:

$$\left. \frac{\partial q_{\text{sat}}}{\partial T} \right|_{(T=T_a)} = \frac{L q_{\text{sat}}(T_a)}{R_v T_a^2} = \beta q_{\text{sat}}(T_a) \tag{A2}$$

where R_v is the gas constant for water vapor. To correctly apply this formula to the model variables, T_a and RH_a should correspond to the first model layer and be computed at the model time step. The fluxes are, however, surprisingly well approximated by the above formulas when considering the climatological annual mean at standard observational levels, i.e., at 2 m for temperature and humidity $T_a = T_{2m}$ and $\text{RH} = \text{RH}_{2m}$ and at 10 m for wind $|V_a| = V_{10m}$, if using an effective coefficient $\gamma^* = 1.7 \times 10^{-3} \times 2.5 \times 10^6$ J/m^3. This choice corresponds to a transfer coefficient for the evaporation $C_E^* \simeq 1.4 \times 10^{-3}$, given that $L = 2.5 \times 10^6$ J/kg and $\rho \simeq 1.2$ kg/m^3 in the tropics. This effective coefficient mitigates the absence of information on the transfer coefficient in the CMIP database (typically of the order of 1 to 1.2 $\times 10^{-3}$), the fact that the 10 m wind is generally weaker than that at the first model layer, the underestimation of the temperature contrast with SST, the difference in relative humidity, and the effects of nonlinearities. This coefficient can also be deduced for each model as the average over the tropical oceans of $L_v H/(C_p \delta T)/|V_a|$. In the supporting information, this formulation is shown to work for each model, both for the computation of the flux itself (Figures S3 and S4) and for the adjustment of latent heat flux to coupling (Figures S5 and S6) ΔLE (Δ refers to the difference historical minus amip) when using $\Delta LE = \Delta LE_{\text{dyn}} + \Delta LE_{\text{sat}} + \Delta LE_{\text{RH}} + \Delta LE_{\delta T}$ with

$$\Delta LE_{\text{dyn}} = \gamma^* \Delta |V_a| q_{\text{sat}}(T_a) \left[\alpha\, \beta\, \delta T + \alpha - \text{RH}\right] \tag{A3}$$

$$\Delta LE_{\text{sat}} = \gamma^* |V_a| \left[\alpha \left. \frac{\partial^2 q_{\text{sat}}}{\partial T^2} \right|_{(T=T_a)} \delta T + \left. \frac{\partial q_{\text{sat}}}{\partial T} \right|_{(T=T_a)} \times (\alpha - \text{RH}) \right] \Delta T_a \tag{A4}$$

$$\simeq \gamma^* |V_a|\, \beta\, q_{\text{sat}}(T_a) \left[\alpha\, \beta\, \delta T + \alpha - \text{RH}\right] \Delta T_a \tag{A5}$$

$$\Delta LE_{\text{RH}} = -\gamma^* |V_a|\, q_{\text{sat}}(T_a) \Delta \text{RH} \tag{A6}$$

$$\Delta LE_{\delta T} = \gamma^* |V_a| \times \alpha \beta q_{sat}(T_a) \Delta \delta T \tag{A7}$$

The same decomposition is also used to compute the contribution of the relative humidity bias to the latent heat flux bias in stand-alone atmospheric simulations, using the difference between the simulated and the observed relative humidity for ΔRH.

Acknowledgments
To analyze the CMIP5 data, this study benefited from the IPSL Prodiguer-Ciclad facility which is supported by CNRS, UPMC, and Labex L-IPSL which is funded by the ANR (grant ANR-10-LABX-0018) and by the European FP7 IS-ENES2 project (grant 312979). The work benefited from a support of the FP7 "Preface" project (grant 603521). We thank Jean-Yves Grandpeix for his help on the manuscript. The figures were generated using the cdo, ferret, and python (scipy.stats.linregress for regression lines) softwares. Both the data and input files necessary to reproduce this study, and in particular the ETO mask, are available from the authors upon request (frederic.hourdin@lmd.jussieu.fr). Finally, we want to thank the two reviewers for their very positive comments and Bjorn Stevens for his feedbacks that helped us reinforce the conclusions of the manuscript.

References

Asrar, G., et al. (2015), Climate symposium 2014: Findings and recommendations, *Bull. Am. Meteorol. Soc.*, *96*, ES145–ES147, doi:10.1175/BAMS-D-15-00003.1.

Braconnot, P., F. Hourdin, S. Bony, J.-L. Dufresne, J.-Y. Grandpeix, and O. Marti (2007), Impact of different convective cloud schemes on the simulation of the tropical seasonal cycle in a coupled ocean-atmosphere model, *Clim. Dyn.*, *29*, 501–520.

da Silva, A., A. C. Young, and C. Levitus (1994), Atlas of surface marine data 1994, volume 1: Algorithms and procedures, *Tech. Rep. 6.*, U.S. Dep. of Commer., NOAA, NESDIS, Washington, D. C.

Dahan Dalmedico, A. (2001), History and epistemology of models: Meteorology (1946–1963) as a case study, *Arch. Hist. Exact Sci.*, *55*(5), 395–422, doi:10.1007/s004070000032.

de Szoeke, S. P., C. W. Fairall, D. E. Wolfe, L. Bariteau, and P. Zuidema (2010), Surface flux observations on the Southeastern Tropical Pacific Ocean and attribution of SST errors in coupled ocean-atmosphere models, *J. Clim.*, *23*, 4152–4174, doi:10.1175/2010JCLI3411.1.

Edwards, P. N. (2010), *A Vast Machine: Computer Models, Climate Data, and the Politics Of Global Warming*, Mit Press, Cambridge, U. K.

Flato, G., et al. (2013), Evaluation of climate models, in *Climate Change 2013: The Physical Science Basis. Contribution of Working Group I to the Fifth Assessment Report of the Intergovernmental Panel on Climate Change*, edited by T. F. Stocker et al., pp. 741–866, Cambridge Univ. Press, Cambridge, U. K., and New York., doi:10.1017/CBO9781107415324.020.

Găinuşă-Bogdan, A., P. Braconnot, and J. Servonnat (2015), Using an ensemble data set of turbulent air-sea fluxes to evaluate the IPSL climate model in tropical regions, *J. Geophys. Res. Atmos.*, *120*, 4483–4505, doi:10.1002/2014JD022985.
Held, I. M. (2005), The gap between simulation and understanding in climate modeling, *Bull. Am. Meteorol. Soc.*, *86*, 1609–1614, doi:10.1175/BAMS-86-11-1609.
Hourdin, F., et al. (2013a), LMDZ5B: The atmospheric component of the IPSL climate model with revisited parameterizations for clouds and convection, *Clim. Dyn.*, *40*, 2193–2222, doi:10.1007/s00382-012-1343-y.
Hourdin, F., et al. (2013b), Impact of the LMDZ atmospheric grid configuration on the climate and sensitivity of the IPSL-CM5A coupled model, *Clim. Dyn.*, *40*, 2167–2192, doi:10.1007/s00382-012-1411-3.
Large, W. G., and G. Danabasoglu (2006), Attribution and impacts of upper-ocean biases in CCSM3, *J. Clim.*, *19*, 2325–2346, doi:10.1175/JCLI3740.1.
Loeb, N. G., B. A. Wielicki, D. R. Doelling, G. L. Smith, D. F. Keyes, S. Kato, N. Manalo-Smith, and T. Wong (2009), Toward optimal closure of the Earth's top-of-atmosphere radiation budget, *J. Clim.*, *22*(3), 748–766, doi:10.1175/2008JCLI2637.1.
Lynch, P. (2008), The origins of computer weather prediction and climate modeling, *J. Comput. Phys.*, *227*, 3431–3444, doi:10.1016/j.jcp.2007.02.034.
Ma, C.-C., C. R. Mechoso, A. W. Robertson, and A. Arakawa (1996), Peruvian stratus clouds and the tropical pacific circulation: A coupled ocean-atmosphere GCM study, *J. Clim.*, *9*, 1635–1645, doi:10.1175/1520-0442(1996)009<1635:PSCATT>2.0.CO;2.
Neggers, R. A. J., J. D. Neelin, and B. Stevens (2007), Impact mechanisms of shallow cumulus convection on tropical climate dynamics, *J. Clim.*, *20*, 2623–2642, doi:10.1175/JCLI4079.1.
Reichler, T., and J. Kim (2008), How well do coupled models simulate today's climate?, *Bull. Am. Meteorol. Soc.*, *89*, 303–311, doi:10.1175/BAMS-89-3-303.
Richter, I. (2015), Climate model biases in the eastern tropical oceans: Causes, impacts and ways forward, *WIREs Clim. Change*, *6*, 345–358, doi:10.1002/wcc.338.
Roehrig, R., D. Bouniol, F. Guichard, F. Hourdin, and J.-L. Redelsperger (2013), The present and future of the West African monsoon: A process-oriented assessment of CMIP5 simulations along the AMMA transect, *Clim. Dyn.*, *26*, 6471–6505, doi:10.1175/JCLI-D-12-00505.1.
Shkolnik, A., C. R. Taylor, V. Finch, and A. Borut (1980), Why do Bedouins wear black robes in hot deserts?, *Nature*, *283*, 373–375.
Stevens, B. (2007), On the growth of layers of nonprecipitating cumulus convection, *J. Atmos. Sci.*, *64*, 2916–2931, doi:10.1175/JAS3983.1.
Taylor, K.-E., D. Williamson, and F. Zwiers (2000), The sea surface temperature and sea-ice concentration boundary conditions for AMIP II simulations, *PCMDI Rep. 60*., Progr. for Clim. Model Diagn. and Intercomparison, Lawrence Livermore Natl. Lab., Livermore, Calif.
Taylor, K. E., R. J. Stouffer, and G. A. Meehl (2012), An overview of CMIP5 and the experiment design, *Bull. Am. Meteorol. Soc.*, *93*, 485–498, doi:10.1175/BAMS-D-11-00094.1.
Vannière, B., E. Guilyardi, T. Toniazzo, G. Madec, and S. Woolnough (2014), A systematic approach to identify the sources of tropical SST errors in coupled models using the adjustment of initialised experiments, *Clim. Dyn.*, *43*, 2261–2282, doi:10.1007/s00382-014-2051-6.
Xu, Z., P. Chang, I. Richter, W. Kim, and G. Tang (2014a), Diagnosing southeast tropical Atlantic SST and ocean circulation biases in the CMIP5 ensemble, *Clim. Dyn.*, *43*, 3123–3145, doi:10.1007/s00382-014-2247-9.
Xu, Z., M. Li, C. M. Patricola, and P. Chang (2014b), Oceanic origin of southeast tropical Atlantic biases, *Clim. Dyn.*, *43*, 2915–2930, doi:10.1007/s00382-013-1901-y.
Yu, J.-Y., and C. R. Mechoso (1999), Links between annual variations of Peruvian stratocumulus clouds and of SST in the eastern equatorial Pacific, *J. Clim.*, *12*, 3305–3318, doi:10.1175/1520-0442(1999)012<3305:LBAVOP>2.0.CO;2.
Yu, L., and R. A. Weller (2007), Objectively analyzed air sea heat fluxes for the global ice-free oceans (1981–2005), *Bull. Am. Meteorol. Soc.*, *88*, 527–539, doi:10.1175/BAMS-88-4-527.
Zheng, Y., T. Shinoda, J.-L. Lin, and G. N. Kiladis (2011), Sea surface temperature biases under the stratus cloud deck in the Southeast Pacific Ocean in 19 IPCC AR4 coupled general circulation models, *J. Clim.*, *24*, 4139–4164, doi:10.1175/2011JCLI4172.1.